iScience

Article

Simultaneous co-delivery of Ginsenoside Rg3 and imiquimod from PLGA nanoparticles for effective breast cancer immunotherapy

Graphical abstract

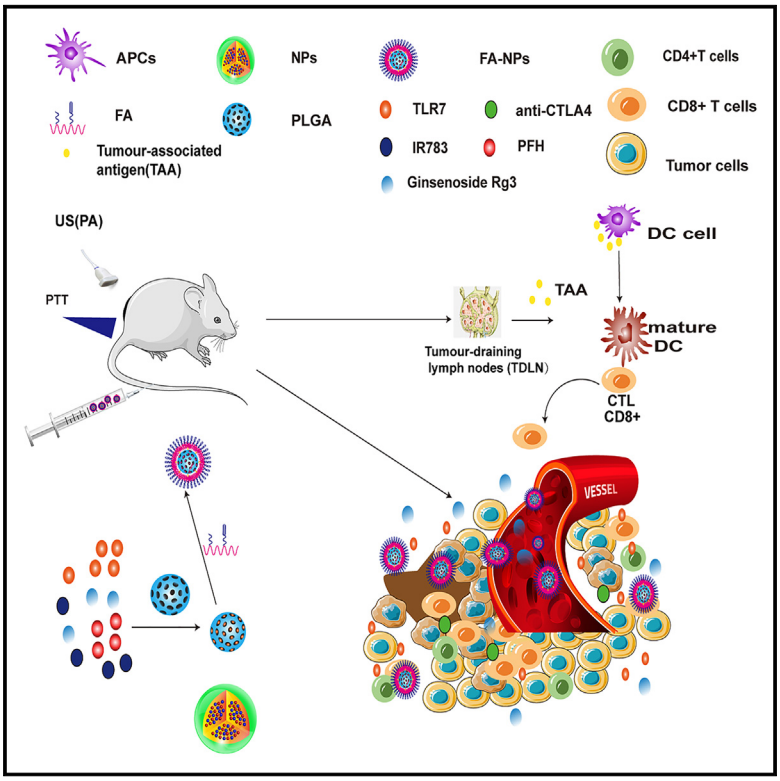

Highlights

- FA-NPs was developed to simultaneous deliver Ginsenoside Rg3 and imiquimod
- FA-NPs can be activated by PTT resulting in anti-tumor effect
- FA-NPs can be used as dual-mode contrast agents for photoacoustic and ultrasound imaging
- FA-NPs provide a strong immune memory effect to prevent tumor recurrence

Authors

Cong Hu, Shuxiong Nong, Qianqian Ke, ..., Qi Zhang, Chilin Liao, Meng Wu

Correspondence

chilinliao@126.com (C.L.), wb000713@whu.edu.cn (M.W.)

In brief

Drug delivery system; Cancer; Biomaterials; Nanomaterials

Hu et al., 2025, iScience *28*, 112274
May 16, 2025
https://doi.org/10.1016/j.isci.2025.112274

CellPress

iScience

CellPress
OPEN ACCESS

Article

Simultaneous co-delivery of Ginsenoside Rg3 and imiquimod from PLGA nanoparticles for effective breast cancer immunotherapy

Cong Hu,[1,4] Shuxiong Nong,[2,4] Qianqian Ke,[1,4] Ziming Wu,[3] Yuancheng Jiang,[1] Ying Wang,[1] Yixin Chen,[1] Ziling Wu,[1] Qi Zhang,[1] Chilin Liao,[2,*] and Meng Wu[1,5,*]

[1]Department of Ultrasound, Zhongnan Hospital of Wuhan University, Wuhan 430071, Hubei, China
[2]Department of Cardiology, Baise People's Hospital. Affiliated Southwest Hospital of Youjiang Medical University for Nationalities, Baise 533000, Guangxi, China
[3]School of Public Health, Southeast University, Nanjing 210009, Jiangsu, China
[4]These authors contributed equally
[5]Lead contact
*Correspondence: chilinliao@126.com (C.L.), wb000713@whu.edu.cn (M.W.)
https://doi.org/10.1016/j.isci.2025.112274

SUMMARY

Breast cancer is a fatal malignancy facing human health, with most patients experiencing recurrence and resistance to chemotherapy. The immunosuppressive tumor microenvironment (TME) greatly limits the actual outcome of immunotherapy. This study aimed to develop a modality of theranostics nanoparticles for breast cancer based on a near-infrared light-triggered nanoparticle for the targeted delivery of ginsenoside Rg3 and immune adjuvants imiquimod (R837) for effective breast cancer immunotherapy. Folate-receptor (FA) targeting IR780-R837/ginsenoside Rg3-perfluorohexane (PFH) @ polyethylene glycol (PEG)—poly (lactide-co-glycolic acid) (PLGA) nanoparticles (FA-NPs) can be activated by near-infrared laser irradiation in tumors, which leads to rapid release of ginsenoside Rg3 and R837 in the regions with high expression of folate receptors and glucose transporter 1 (GLUT1). Meanwhile, the nanoparticles can be used as dual-mode contrast agents for photoacoustic and ultrasound imaging. This strategy provides a strong immune memory effect, which can prevent tumor recurrence after eliminating the initial tumor.

INTRODUCTION

Breast cancer has a high degree of malignancy, poor prognosis, and a high incidence rate among women.[1] Traditional treatment for breast cancer includes surgery, chemotherapy, and radiotherapy but their effectiveness is often limited, and recurrence is not uncommon. Finding an efficient treatment strategy to eliminate tumors with low toxicity and prevent recurrence is the ultimate goal of cancer treatment. In recent years, with the continuous development of nanomedicine, research has shown that nanoparticles can play a role in killing tumors and interacting with the immune system.[2–4] Nanoparticles can be utilized to stimulate the innate immune system to attack tumor cells, demonstrating great potential as targeted tumor therapies.[5] They were expected to become a new tool for the next generation of breast cancer treatment.

Breast cancer immunotherapy has seen significant advancements in recent years, with a focus on leveraging the body's immune system to target and eradicate tumor cells. Research is exploring the potential of making the tumor microenvironment (TME) of hormone receptor-positive (HR+)/HER2-negative breast cancer more immunologically "hot" through immunotherapy-based combination regimens. Immune checkpoint inhibitors (ICIs) have shown promising efficacy in triple-negative breast cancer (TNBC), with atezolizumab and pembrolizumab being notable examples. Pembrolizumab combined with nanoparticle albumin-bound (nab)-paclitaxel is the standard first-line therapy for patients with metastatic TNBC who have a PD-L1-positive peritumoral immune infiltrate. Breast cancer chemotherapy drugs like adriamycin and docetaxel can induce side effects, such as nausea, diarrhea, hair loss, immunosuppression, fatigue, and anemia. Currently, various types of cancer immunotherapy, including cytokine therapy, checkpoint blockade therapy, and cancer vaccines, have been widely applied, showing promising clinical results.[6–10] However, most of these immunotherapy strategies have drawbacks such as high cost, variations in individual treatment responses, and immunotoxicity, such as cytokine release syndrome.[11–13] Cancer vaccines have unique advantages in cancer immunotherapy methods. They can induce antigen-specific expression and tumor specific immunity due to the presence of tumor-associated antigens (TAAs), rather than the non-specific immune responses in checkpoint blockade therapy.[7] Additionally, cancer vaccines can provide long-term immune memory, which can help prevent cancer recurrence. TAAs, such as specific proteins or peptide adjuvants, can induce strong anti-tumor immunity, but their

heterogeneity in patient tumors limits their clinical application.[14] In contrast, whole-cell cancer vaccines (such as those from dissected tumor lysate tissue) can induce immunity to all tumor antigens and can be applicable to various types of solid tumors. However, the complexity of the entire preparation process and the uncertainty surrounding vaccine dosage has resulted in unsatisfactory clinical outcomes for cancer cell vaccines to date. Therefore, researching a simple, efficient, and specific cancer immunotherapy has become a new direction for research.[2,15,16] Photothermal therapy (PTT) is an emerging treatment method that uses light-absorbing agents to generate heat and ablate tumor cells at the tumor site.[17,18] Drawing inspiration from these intriguing research findings, we designed an *in situ* immune adjuvant nanoparticle following tumor photothermal ablation. The ablated TAAs produced a tumor vaccine-like immune response, demonstrating a strong anti-tumor immune response.

Ginsenoside Rg3, derived from ginseng, is an active compound approved for clinical cancer treatment, including breast cancer.[19] However, its susceptibility to degradation in the gastrointestinal tract and blood, coupled with its poor water solubility, often necessitates the use of non-ionic surfactants, which could potentially lead to adverse reactions like allergies and peripheral neuropathy.[20–22] Nanocarriers offer a promising solution to these challenges. Cancer cells often exhibit heightened glucose uptake to satisfy their increased metabolic demands. Glucose transporter 1 (GLUT1) is the predominant facilitator of glucose uptake in these cells, with its expression markedly higher in cancer cells compared to normal cells.[23] Leveraging this, GLUT1 has emerged as a clinically validated target for drug delivery, particularly in tumor models. Ginsenosides, being established substrates for GLUT1 and the sodium-coupled glucose co-transporter 1 (SGLT1), can enhance the targeting of nanoparticles to tumors with elevated expression of these transporters.[24,25] Poly (lactic-co-glycolic acid) (PLGA), composed of lactic acid (LA) and glycolic acid (GA) units, is a biodegradable, high-molecular-weight polymer with attributes of degradability, biocompatibility, low toxicity, and non-immunogenicity. PLGA nanoparticles also capitalize on their enhanced permeability and retention (EPR) effect, promoting accumulation in tumor regions. These features have solidified PLGA's role in medical applications as a scaffold or carrier material. Administering the PLGA drug delivery system intravenously can boost the concentration of ginsenoside Rg3 within the tumor, thus extending its half-life and improving bioavailability, which is crucial for precise cancer therapy.

In our formulation, these nanoparticles components consist of: poly (lactide-co-glycolic acid) (PLGA) as the encapsulation polymer, ginsenoside Rg3, IR780, imiquimod (R837), and PFH. The loading process of nanoparticles mainly takes advantage of two characteristics: a low boiling point (56°C) and ability to transition from liquid to gaseous phase, thus transforming nanoparticles into microbubbles when triggered with light irradiation, thereby enhancing the ultrasound echo which is useful for ultrasound contrast.[26] IR780, as a photosensitizer for NIR light irradiation, can effectively convert light into heat which a form of PTT for the destruction of cancer cells.[27–29] Folic acid is a human B vitamin and micronutrient which interacts with folic acid receptors through ligand receptor-binding.[30] Folic acid receptors are overexpressed on various solid tumor cell membranes, including breast cancer, lung cancer, and prostate cancer.[31] Folic acid-modified nanoparticles can target folate receptor overexpressing cells, achieving targeted binding to cancer cells and targeted drug release.[32–35] Imiquimod (R837) can promote dendritic cells (DCs) maturation and intra-tumoral infiltration of $CD8^+$ T cells. In this study, we applied PLGA NPs not only as an anti-cancer therapy but also for diagnostic imaging. It was hypothesized that the folate on the surface of the NPs would contribute to the selective binding of the NPs to folate-receptor-positive cancer cells, leading to enhanced targeted binding and anticancer efficacy via a laser-triggered drug-delivery system combined with PTT. Meanwhile, owing to the excellent PA imaging and the ability of PFH to phase-change, the NPs could serve as a dual-modality contrast agent for PA and US imaging.

RESULT

Basic characteristics

Under transmission electron microscopy, FA-NPs appeared as uniformly sized circular shapes (Figure 1A); Scanning electron microscope observation showed spherical shapes (Figure 1A), with a particle size of 150.4 ± 11.4 nm (Figure 1A), with a potential of −16.3 ± 3.79 (Figure 1B), and with good stability for 7 days. The loading capacity of ginsenoside Rg3/R837 has been confirmed by HPLC, and the encapsulation efficiency was 34.3%, while R837 was 38.5%. After absorbing light energy, IR780 converts the light energy into thermal energy, causing a sharp increase in the local temperature of the nanoparticles. This high temperature transforms phase-changing PFH into a gaseous state, which is sufficient to disrupt the biological structure of the nanoparticles, leading to their rupture (Figure 1C). Intact particles have a consistent size and shape, while ruptured particles have irregular shapes and sizes. Intact particles may be more stable than ruptured ones, which can aggregate or settle out of suspension more quickly. In the case of drug-delivery nanoparticles, rupture could potentially result in a faster or more erratic release profile of the drug from ruptured particles. Ruptured particles could have different cytotoxic effects on cells compared to intact particles, potentially due to the release of internal contents or changes in surface chemistry. Release of ginsenoside Rg3 from the FA-NPs with or without laser irradiation was shown (Figure 1D). The PLGA nanoparticles labeled with Dil dye showed uniformly distributed red particles under laser confocal microscopy. The folate target was modified with FITC labeling, and the nanoparticles and folate were co-localized under fluorescence microscopy (Figure 1E). The results showed that the nanoparticles and folate were fluorescence aligned, indicating that folate was successfully connected to PLGA. Photoacoustic imaging is a non-invasive imaging technique that combines the high contrast of optical imaging with the deep penetration capabilities of ultrasound imaging. When nanoparticles absorb photonic energy and convert it into thermal energy, it causes rapid thermal expansion of the surrounding medium, generating ultrasound waves. These ultrasound waves can be detected and used for imaging, which is known as photoacoustic imaging. The B-mode photothermal effect and PA signals provide a method for assessing and optimizing nanoparticles for

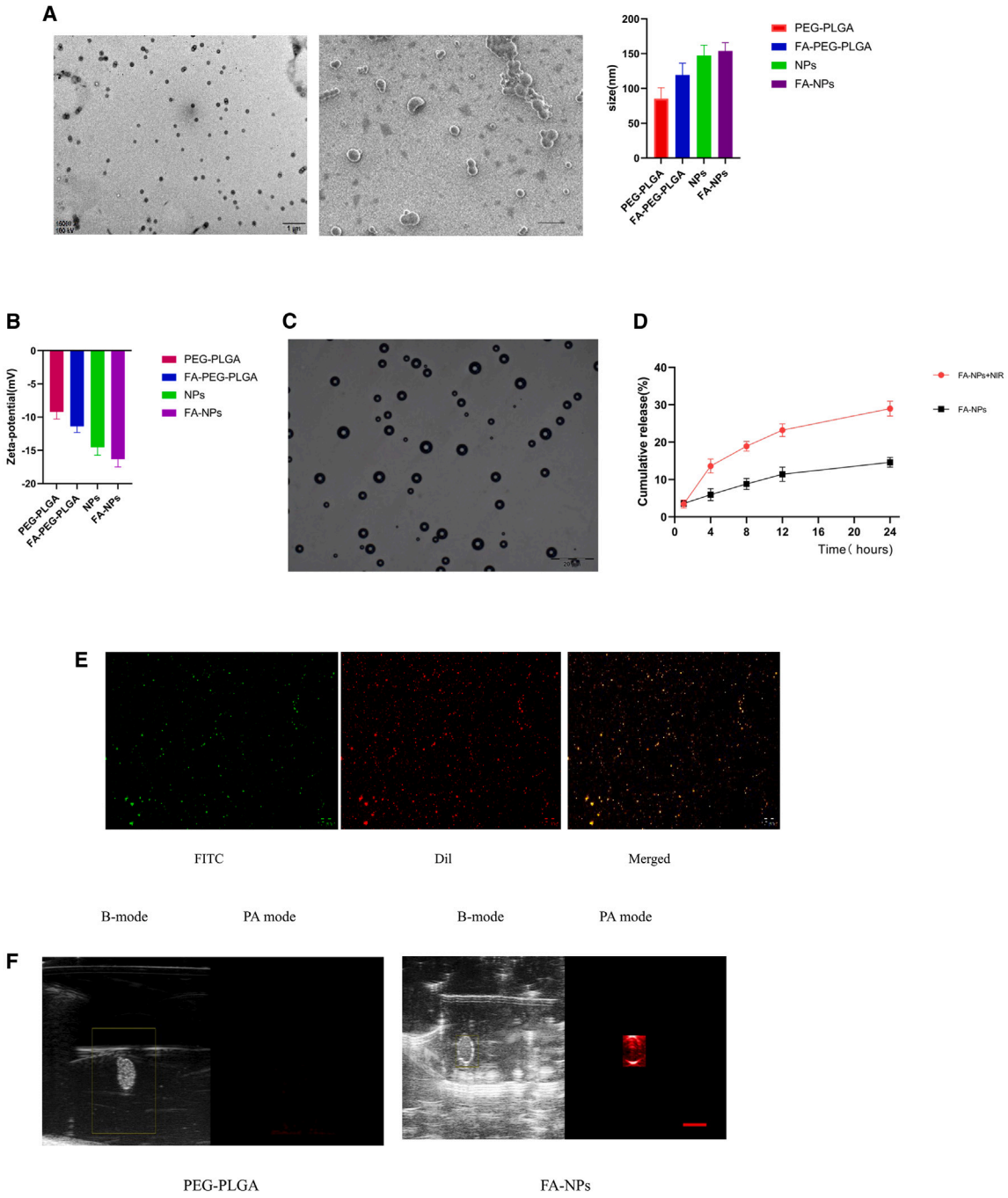

Figure 1. Characterization of FA-NPs, NPs

(A) TEM and SEM images and size distribution of PEG-PLGA, FA-PEG-PLGA, FA-NPs, NPs, scale bars, 1 μm.

(B) Surface zeta potential of nanoparticles was determined by DLC (n = 3).

(C) Optical microscopy images of phage change of FA-NPs. Scale bars, 20 μm.

(D) Release behavior of ginsenoside Rg3 from the FA-NPs with or without laser irradiation (E) DiI-labeled NPs (red), FITC-labeled folate(green) by covalently coupling reaction, overlapping the folate using the NPs emerging as yellow fluorescence in the mixed channel. Scale bars, 20 μm.

(F) B-mode photothermal effect and PA signals *in vitro* under the 808 nm laser (5 min, 1 W/cm^2) irradiation in phantom gel model, Scale bars, 1 cm.

diagnostic and therapeutic applications for *in vitro* experiments. By observing B-mode photothermal effects and PA signals under laser irradiation in a gel model, it was found that the PA intensity of the nanoparticles increased, indicating a good photothermal effect (Figure 1F).

In vivo multimodal imaging

In the field of multimodal imaging, the combination of photoacoustic imaging and ultrasound imaging offers a powerful tool capable of acquiring morphological, functional, and molecular information about biological tissues simultaneously. The integrated multimodal imaging system, which combines photoacoustic imaging and ultrasound imaging, is capable of delineating dense vascular networks and hemodynamic and morphological changes in both superficial and deep tissues. A key advantage of this system is its ability to provide complementary tissue information from different imaging modalities. Ultrasound imaging displayed FA-NPs after PTT irradiation, showing that echoes in both B mode and contrast mode gradually increased with the strongest echo intensity observed at 15 min (Figure 2A). Photoacoustic imaging showed that the signal of FA-NPs was enhanced compared to NPs (Figure 2B). Ultrasound results showed that the nanoparticles could enter the mice tumor area. This study integrates photoacoustic imaging with ultrasound imaging to provide a multimodal map that offers rich biological information, aiding in the diagnosis of breast cancer and guiding treatment plans. The successful preparation of these multimodal imaging nanoparticles holds potential for future clinical translation and application in breast cancer management.

In vitro targeting

After co-incubation of 4T1 cells with both NPs and FA-NPs nanoparticles for 24 h, the cell survival rates were all above 90% (Figure 4A). Confocal imaging displayed that in the FA-NPs group, a large number of nanoparticles aggregate around the cell membrane and within the cytoplasm. In contrast, only a small amount of nanoparticle aggregation was observed around the cell membrane in the NPs group (Figure 3A), and the binding was measured by flow cytometry (Figure 3B), followed by confocal microscopy (Figure 3A).

4T1 cells apoptosis assays and CCK-8 assays

Previous studies have shown that nanoparticles combined with photothermal agents (PTAs) can achieve tumor ablation capabilities. PTT utilizes PTAs to convert light energy into heat energy under near-infrared irradiation to kill tumor cells.[36–38] PTAs absorb photon energy under NIR irradiation and, through nonradiative decay-relaxation, cause the surrounding microenvironment to heat up, generating a thermal effect. *In vitro* experiments have already demonstrated that tumor cells treated with IR780 nanoparticles show significant cell death under 808 nm laser irradiation, and the cell survival rate decreases with increased nanoparticle concentration and prolonged irradiation time.[37,38] CCK8 test results showed the survival rate of 4T1 cells in the FA-NPs +NIR group was lower than that of the FA-NPs group, both of which were lower than the control group (Figure 4A). There was no statistically significant difference between the other groups and the control group. Flow cytometry showed significant 4T1 cell apoptosis in the FA-NPs +NIR group and NPs +NIR groups. The rate of cell apoptosis in other groups is relatively low. The results demonstrated the photothermal ablation capability of FA-NPs (Figure 4B). Under 808 nm laser irradiation, FA-NPs possess superior capabilities in achieving tumor ablation capabilities.

Animal experiments

Following two weeks of habituation, 4T1 tumor cells, at a concentration of 5×10^5, were injected into the left flank of the mice to initiate tumorigenesis. The subcutaneous breast cancer tumor model of mice was divided into different groups for treatment. To evaluate synergistic anticancer efficacy further, tumor volumes were measured every 3 days and normalized against their original volume. The PBS and PEG-PLGA groups each showed a 6-fold increase in average tumor volume when compared with the FA-NPs + NIR group (Figure 5A), and there was no significant difference between the PBS and PEG-PLGA groups, indicating that 4T tumor growth was not affected by PEG-PLGA alone. Some studies have indicated that the use of laser irradiation alone on tumors may not result in the reduction of tumor size in mice.[38–40] The effectiveness of PTT depends not only on laser irradiation but also on the presence of photothermal agents (PTAs) which convert light energy into heat energy under laser irradiation, effectively killing tumor cells. Without PTAs, laser irradiation alone may not be sufficient to cause tumor killing. Therefore, PTT typically requires the combined use of photothermal agents and laser irradiation to achieve therapeutic effects. Fluorescence imaging and electron microscopy observation of mice tumor tissue showed that nanoparticles had reached localization to the tumor site, but FA-NPs showed more obvious targeting (Figures 5B and 5C). The imaging results of mice tumor tissue indicated that FA-NPs achieved better targeting at the tumor site.

Stimulation of immune response by nanoparticles

Dendritic cells (DCs), as the primary antigen presentation, play a crucial role in initiating and regulating innate and adaptive immune responses. Immature DCs will engulf exposed antigens during their growth process, then process them into peptides and migrate to nearby lymph nodes. Immature DCs will transform into mature DCs and present the main histocompatibility complex peptides, which activate T cells through their corresponding receptors. Therefore, we investigated the effect of FA-NPs nanoparticles on immune function in BALB/c mice with subcutaneous 4T1 tumors by injection of FA-NPs by tail vein. The mice were then irradiated with an 808 nm laser with a power density of 1 W/cm^2 for 5 min while monitoring by ultrasound. Under laser irradiation, the surface temperature of the tumors in the FA-NPs group rapidly rose to 60°C, which was sufficient to effectively kill tumors. By analyzing the DCs status of tumor-draining lymph nodes in treated mice tumors, it will recruit more DCs to the initial tumor site after PTT in FA-NP + NIR group.

$CD8^+$ cytotoxic T lymphocytes (CTL) can directly kill targeted cancer cells, whereas $CD4^+$ helper T cells play important roles in the regulation of adaptive immunities. In this study, PEG-PLGA injection alone failed to promote $CD8^+$ CTL infiltration. In contrast, the percentage of $CD8^+$ CTL after the FA-NPs based

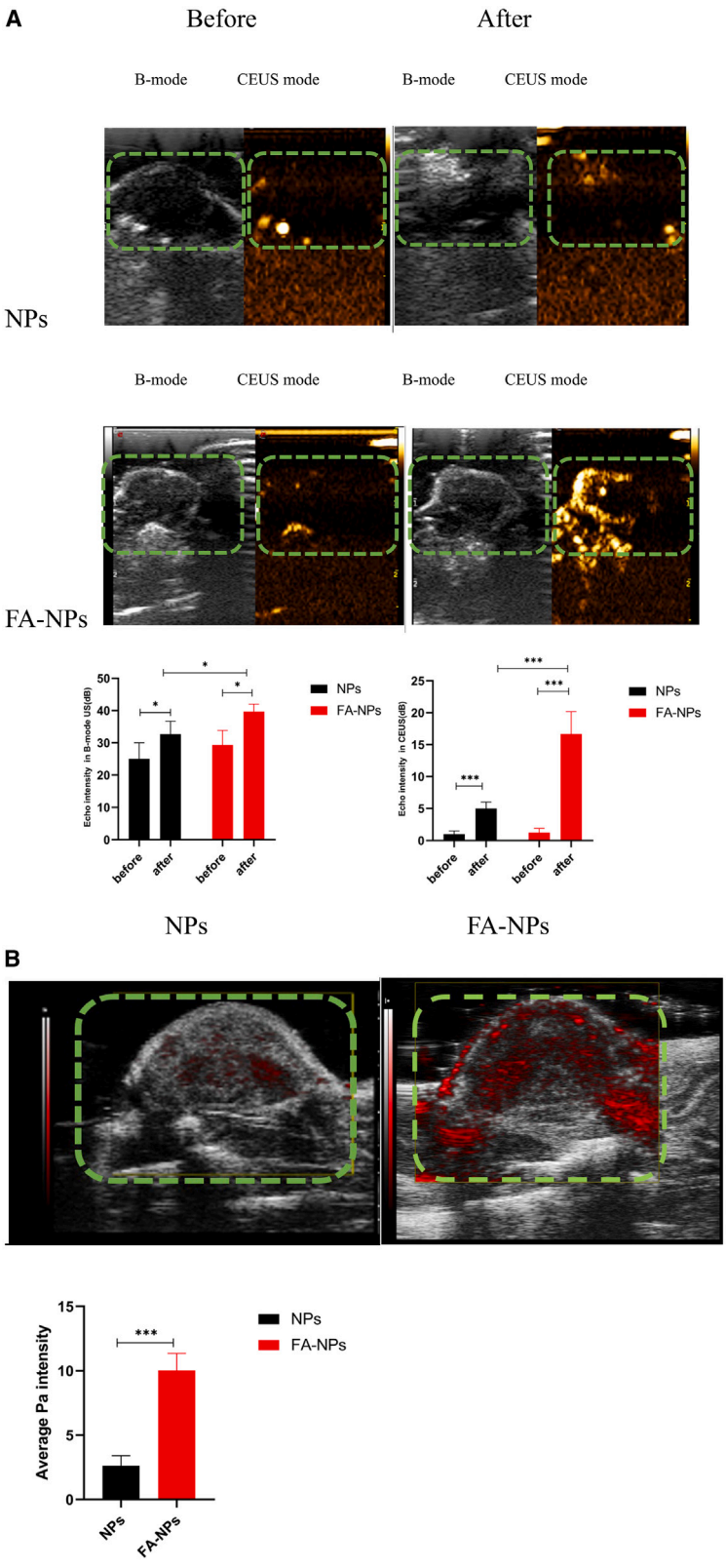

Figure 2. Ultrasound photoacoustic imaging of tumors in mice

(A) PA imaging of before and after 15 min of intravenous injection with FA-NPs and NPs accumulation in 4T1 tumor-bearing mice, Data are represented as mean ± SEM.

(B) US monitoring of NIR laser irradiation 1 h after intravenous injection of FA-NPs and NPs in 4T1 tumor-bearing mice. An illustration of the tumor area in the mice is shown within the dashed lines. Data are represented as mean ± SEM. $^{*}p < 0.05$, $^{***}p < 0.001$ compared with others.

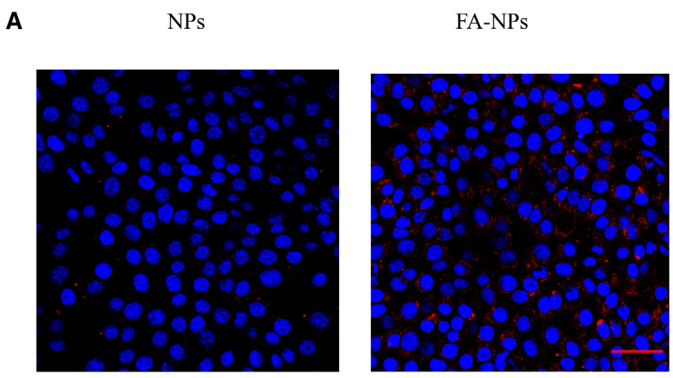

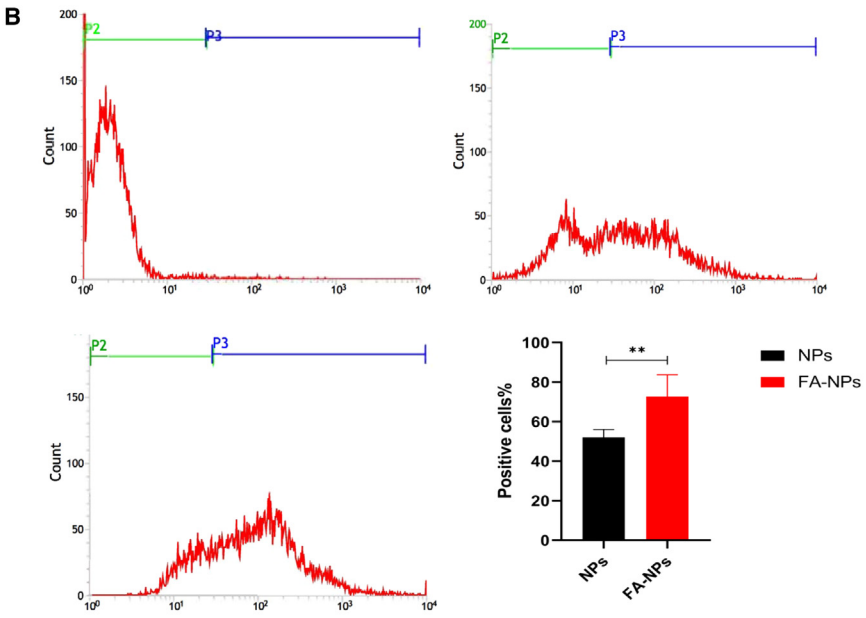

Figure 3. Target binding *in vitro*

(A) Fluorescence imaging, confocal imaging of FA-NPs and NPs to 4T1cells. Blue (DAPI) is a representation of cell nuclei, and the red (Dil) dots show Dil-labeled NPs. Scale bars, 10 μm.

(B) together with the FCM, was used for evaluating the targeting efficacy of FA-NPs and NPs to 4T1cells. Data are represented as mean ± SEM. $^{**}p < 0.01$, compared with others.

PTT treatment significantly increased to 20.8%, which appeared to be higher than that in FA-NPs group without PTT (11.2%) or R837 treatment (12. 6%) (Figure 6 A, 6B). After treatment, the mice were euthanized, and tumor-draining lymph nodes were collected for co-staining with CD11c, CD80, and CD86 using flow cytometry after surgery. Lymph-node derived DCs isolated from BALB/c mice were analyzed to identify the upregulated molecules CD80 and CD86 as co-stimulatory factor DC markers. Compared to the same dose of R837, FA-NPs significantly promoted the maturation of DCs (Figure 6C, 6D). The percentage of mature DCs ($CD11c+CD80^{+}CD86^{+}$) increased to 69.2% after NIR treatment, while mature DCs increased to only 48.1% with free R837 (same dose) treatment. Moreover, the percentage of $CD8^{+}$ T cells in the tumor tissue also showed a remarkable increase in FA-NPs + NIR group (Figure 6G). The percentage of positive TUNEL cells in the FA-NPs +NIR group was also significantly higher than in other groups (Figure 6 E, F). FA-NPs + NIR group exhibited stronger *in vivo* immune stimulation effects, DCs matured and secreted various cytokines to regulate other types of immune cells (Figures 6A, 6B, 6H). In cancer immunotherapy, various cytokines play complex and crucial roles. Interleukin-6 (IL-6) is a pleiotropic cytokine that significantly contributes to hematopoiesis and inflammation. Within the immune response, while it is well-known for its pro-inflammatory characteristics during acute inflammation, the chronic secretion of IL-6 can lead to chronic inflammation, positioning IL-6 as a central player in the promotion and maintenance of cancer. In various types of cancer, high levels of circulating IL-6 are associated with poor survival rates. IL-6 is commonly linked to tumor promotion and immunosuppression.[41] Tumor Necrosis Factor-alpha (TNF-α) is a cytokine capable of directly inhibiting tumor cell growth or indirectly by stimulating the cytotoxic activity of immune cells against tumor cells. TNF-α also participates in the inflammatory response within the TME and may affect tumor development and immune evasion through various mechanisms.[42] Interleukin-12 (IL-12) is a key cytokine that promotes the differentiation of Th1 cells and enhances cell-mediated immune responses. In cancer immunotherapy, IL-12 stimulates the production of IFN-γ, which is crucial for the anti-tumor immune response.[43] Various cytokines, including IL-6, TNF-a, and IL-12 were analyzed using ELISA in each group of mice. IL-12 levels and IL-6 and TNF-a levels in the serum of the FA-NPs treated mice were significantly higher than those in control group and mice treated with the same dose of free R837 (Figure 6H). This observed stronger immune stimulating effect *in vivo* than with free R837 may be attributed to the sustained release of R837 from nanoparticle drugs. These results indicated that FA-NPs can significantly promote the immune response to tumor related-antigens by antigen presentation compared to free R837.

In a murine model, 4T1 breast cancer cells were initially inoculated on the left flank, followed by the inoculation of a

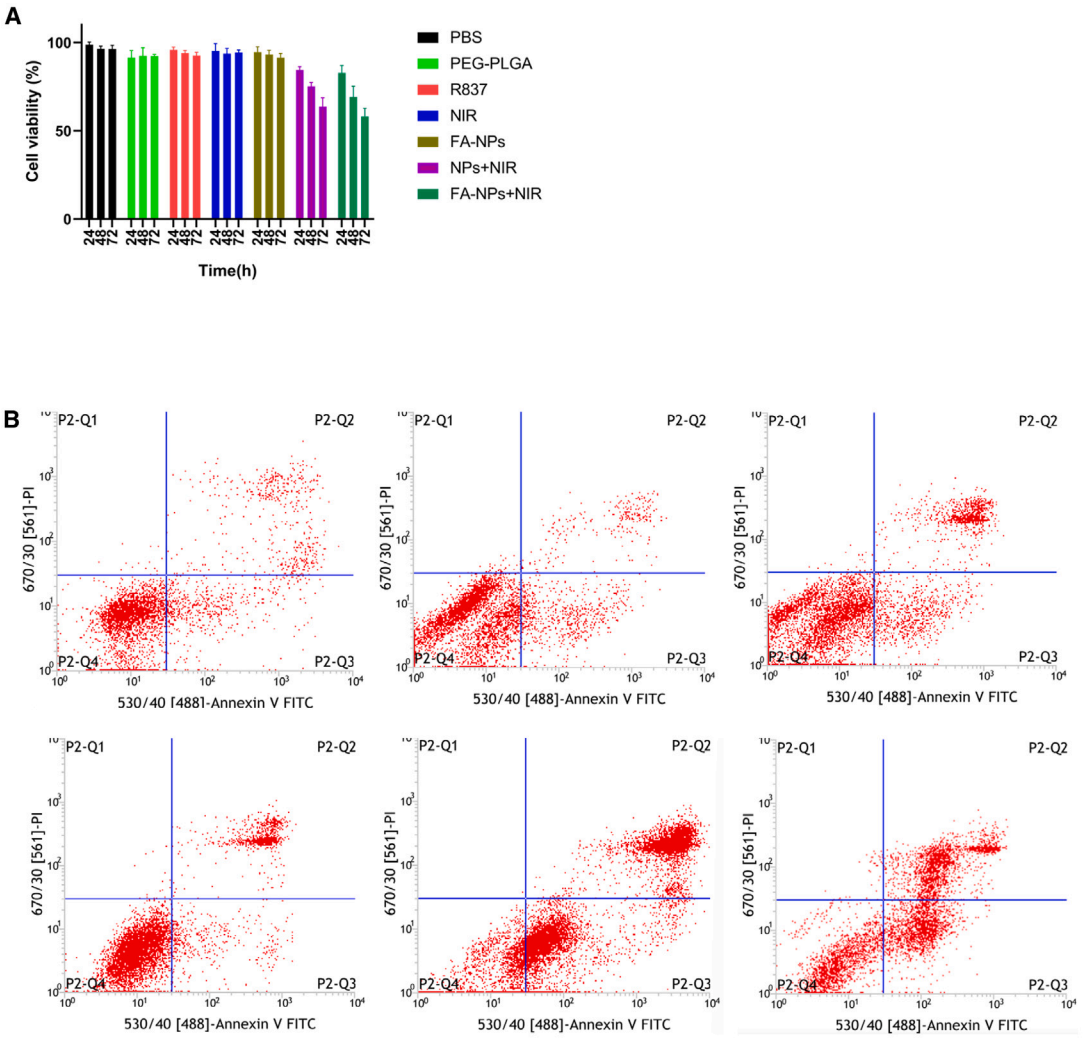

(legend on next page)

secondary tumor on the right flank 1 week later, serving as an artificial simulation of a secondary tumor model. On the subsequent day, the primary tumor on the left flank was subjected to either PTT or surgical excision, as per the experimental group allocation. Subsequently, the mice were administered intravenous injections of anti-CTLA4 (clone 9H10) on days 1, 4, and 7, with a dosage of 10 mg per mouse per treatment.[39] Thereafter, the progression of secondary tumors across different groups was monitored every 2 days using caliper measurements (Figure 6I). It was observed that post-surgical resection of the primary tumor, the secondary tumors exhibited rapid growth. Mice treated with FA-NPs or anti-CTLA4 alone showed a modest reduction in tumor growth rate, whereas the combination of FA-NPs PTT with anti-CTLA4 treatment markedly decelerated the growth of secondary tumors. These findings from the secondary tumor model suggest that the non-specific combined immunotherapy approach is effective in managing the progression of breast cancer metastases. Close surveillance of the mice post-treatment revealed that the mice receiving PTT following FA-NPs administration, in conjunction with CTLA4 blockade, demonstrated significant suppression of cancer metastasis. In comparison to various control groups, where the majority or all mice succumbed to spontaneous metastasis within 60 days, the integration of FA-NPs-based PTT with anti-CTLA4 therapy elevated our survival rate to 70% during a 90-day observation period (Figure 6J). Consequently, the synergistic application of FA-NPs photothermal ablation for primary tumors, alongside anti-CTLA4 therapy, can potently inhibit cancer metastasis and prolong the survival of mice.

DISCUSSION

Chemotherapy is one of the traditional treatment methods for malignant tumors, but it often comes with unavoidable toxic side effects.[29] Ginsenoside Rg3 possesses a variety of functional activities, including inhibiting tumors, anti-metastasis, anti-carcinogenesis, hepatoprotection, neuroprotection, and immune system stimulation.[44–48] Despite the fact that herbal medicines have been used to treat various diseases for centuries, there is still a long way to go in terms of pharmaceutical optimization of their extracts. Ginseng, known as the king of traditional Chinese medicine, has been used for medicinal purposes for thousands of years. Ginseng contains a multitude of types of ginsenosides.[49] Among these ginsenosides, Rg3 has been reported to have potent anti-proliferative and anti-metastatic activities against various types of cancer, including skin cancer, colon cancer, breast cancer, and prostate cancer.[50–52] This includes research findings on the anti-cancer mechanisms of ginsenoside Rg3, its inhibitory and cytotoxic effects on tumor cell lines, as well as its role in immune regulation and apoptosis.[46–48,52]

PTT was a non-invasive tumor treatment method with broader application prospects. Research has shown that nanoparticles can effectively improve the effectiveness of PTT.[52–55] In recent years, PTT has been explored to improve the efficacy of drug delivery for intra-tumoral lesions.[52–55] As a photosensitizer, IR780 exhibits strong absorption in the near-infrared region. PLGA nanoparticles are widely used in photoacoustic imaging, magnetic resonance imaging, and ultrasound imaging, providing high contrast and spatially resolved images.[54–56] This study evaluated FA-NPs photoacoustic, ultrasound, and multimodal imaging capabilities, as well as its effectiveness in combination with PTT therapy for tumors. In this study, a phase change material (PFH) was prepared to combine tumor cell targeting ability with multimodal imaging. PFH can undergo acoustic phase transition and produce microbubbles after ultrasound irradiation, which not only enhances ultrasound imaging but also facilitates the penetration of nanoparticles into the deep part of the tumor to enhance therapeutic efficacy.[30,31] The research leverages the innovative use of PFH, a phase change material that enhances the targeted delivery of drugs from PLGA, particularly in tumor regions. This material not only facilitates the precise deposition of therapeutic agents but also generates gas within the PLGA matrix upon phase transition. The resulting microbubbles within the PLGA structure enable ultrasound-guided diagnostic imaging of the tumor and allows for the real-time tracking of drug delivery. This integrated approach provides a strategy for both theranostics and targeted drug release.

The immunosuppressive TME greatly limits the actual outcome of immunotherapy.[57] Cytotoxic $CD8^+$ T cells (CTLs) are the elite soldiers in the immune system's fight against cancer.[58] Their activation typically occurs through antigen-presenting cells (APCs, such as DCs), seize and exhibit TAAs to primary T cells. DCs in activating T cells are significantly determined by their stage of maturation. Yet, the immunosuppressive grip of the TME frequently maintains DCs in an immature state, rendering them nonfunctional and thus greatly limiting their capacity to spark an immune reaction. Studies have demonstrated that toll-like receptor (TLR) agonists are capable of inducing DC maturation, thereby rejuvenating their functional potential by activating TLRs present on their surface.[52–55] The TLR agonist's limited application might be attributed to the systemic distribution of these low molecular weight agents following local injection, which can incite broad pro-inflammatory reactions and severe immune-mediated adverse effects. Therefore, it is imperative to localize the immunostimulatory impact of these agonists to a confined area, circumventing systemic inflammation and its potential toxicities.[32] The study provided a scientific basis for the potential application of ginsenoside Rg3 and TLR agonist in the treatment of breast cancer in this research topic.

The nanoparticles generated in the study were spherical and uniform in size. This experiment utilized laser irradiation to

Figure 4. Cell apoptosis, cell viability *in vitro*

(A) 4T1 cell viability was measured with CCK-8 after treatment for 24, 48, and 72 h

(B) Apoptosis of 4T1 cells was detected by flow cytometry after treatment for 72 h in different groups. Six groups from left to right are PBS, PEG-PLGA, R837, FA-NPs, NPs +NIR, FA-NPs +NIR.

(C) Quantitative flow cytometric analysis of the percentage of cell apoptotic changes after treatment for 72 h, Data are represented as mean ± SEM.*$p < 0.05$, **$p < 0.01$, ***$p < 0.001$ compared with others.

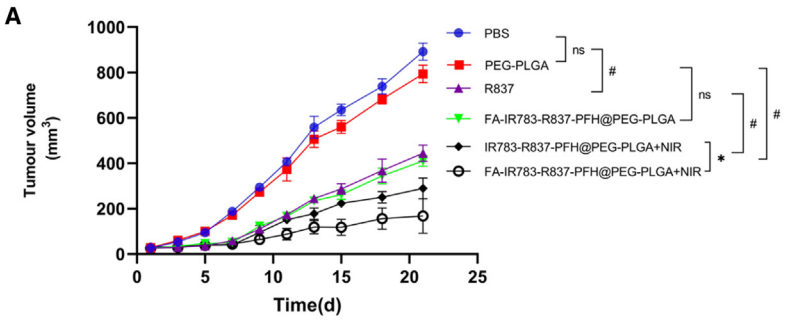

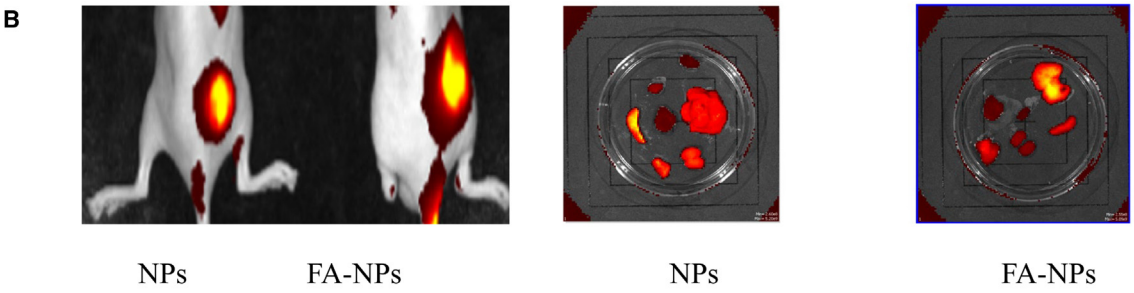

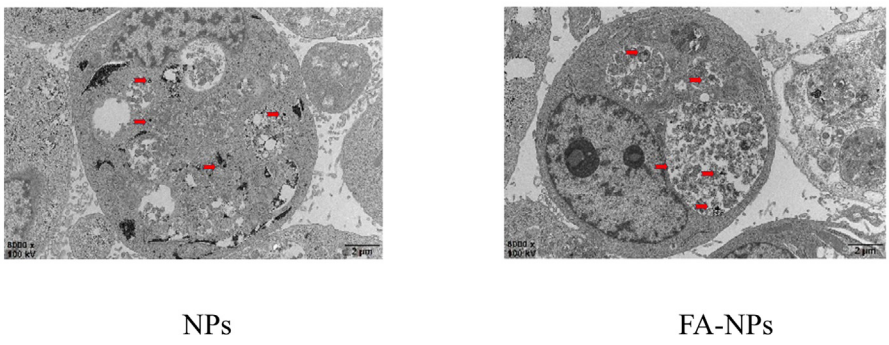

Figure 5. Therapeutic effects in various treatment groups *in vivo*

(A) Tumor volume growth curves in various treatment groups. Data are represented as mean ± SEM.

(B) Fluorescence imaging and bio-distribution in the xenograft tumors. Variations that happen in the fluorescence intensity of DiR-labeled tumors in mice at the 1 h, and fluorescence intensity of main organs and tumors (top left corner in picture) after 24 h after injection of NPs and FA-NPs.

(C) TEM images of FA-NPs and NPs (seen as black dots on the image) in tumor tissue. Red arrows are shown in TEM images of nanoparticles and conjugated nanoparticles. Scale bars, 2 μm. *$p < 0.05$, #$p < 0.001$ compared with other.

induce a liquid gas phase transition in the PFH of the PLGA nanoparticle core, causing the nanoparticle to expand and rupture, thereby releasing internal drugs. Drug release experiments found that the release rate of R837 significantly increases when the nanoparticles are irradiated with a laser, indicating that lasers can stimulate the release of R837 drugs. The results of confocal microscopy show that FA-NPs aggregated more and faster in 4T1 cells than in the control group, indicating its strong 4T1 cell targeting ability. *In vivo* imaging showed FA-NPs had higher accumulation in 4T1 tumors than with NPs after intravenous injection. After 24 h of intravenous injection of FA-NPs, local photothermal ablation was performed on the tumor by irradiating with an 808 nm laser for 5 min (1W/cm^2), causing the surface temperature of the tumor to rise to 60°C. To further explore the

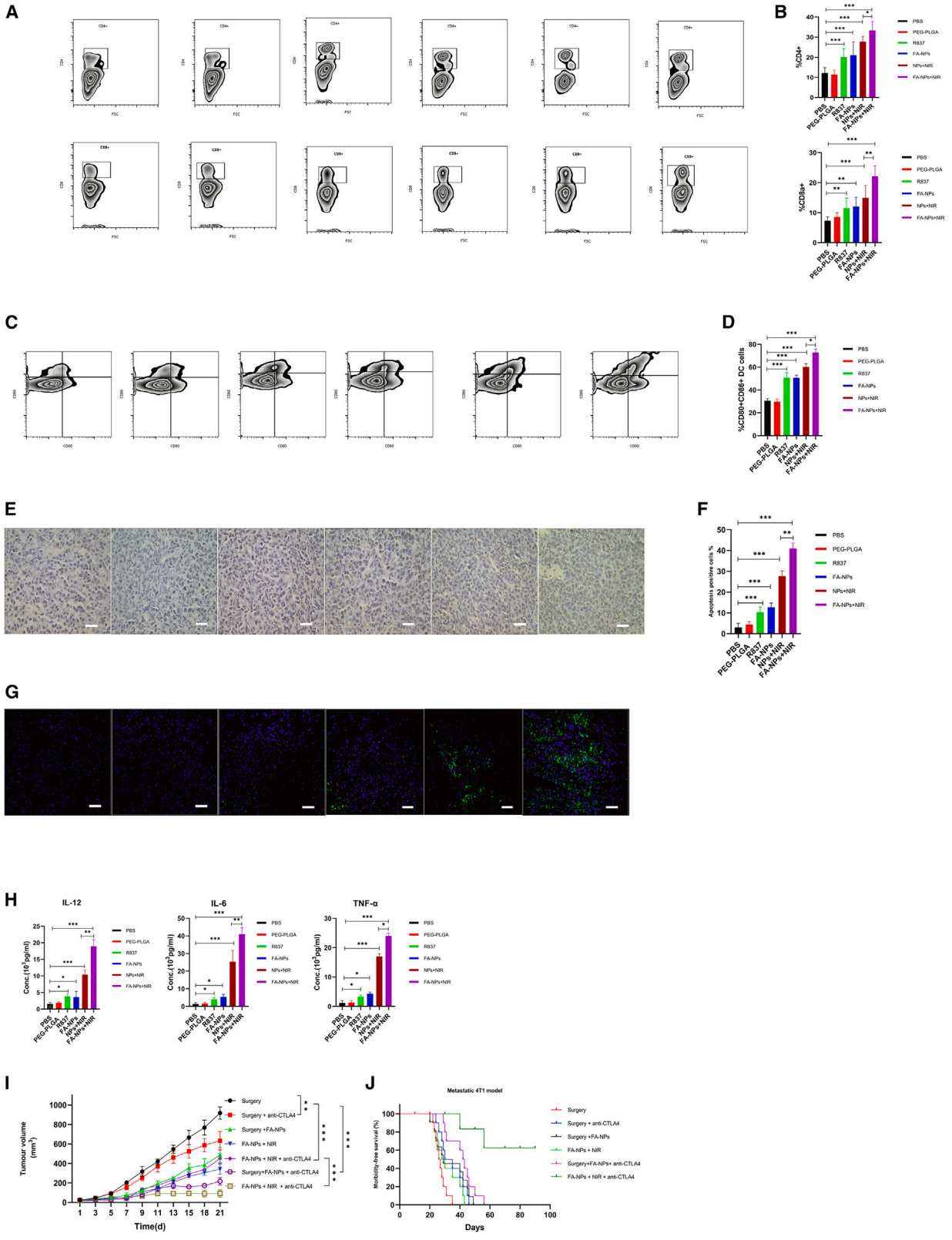

(legend on next page)

immune effects induced by PTT, and mice were intravenously injected with various drugs in the treatment groups, mice lymph nodes were collected and evaluated for the activation of DCs in each group. Serum was collected from each group of mice and analyzed for changes in various cytokines. The results indicated that intravenous injection FA-NPs can induce high maturation of DCs with PTT and enhance the secretion of various key pro-inflammatory cytokines. After injecting with nanoparticles, we did not observe cytokine storm-like side effects, and all mice exhibited normal behavior. After treatment, there was no significant fluctuation in weight or accidental death. Although further careful evaluation of safety is still needed, the therapeutic effect of nanoparticles has great clinical application value, especially for tumors that are difficult to treat through local injection.

Ablative tumor treatments, such as hyperthermia, photodynamic therapy, and cryoablation, can cause strong tumor-specific immune responses.[52–55] Compared with existing immunotherapy strategies, FA-NPs photothermal immunotherapy involved using immune-assisted nanoparticles for photothermal tumor ablation, combined with checkpoint blockade therapy, which may overcome the postoperative recurrence and metastasis issues in traditional cancer immunotherapy. Compared with proteins or peptides that use specific conventional cancer vaccines as antigens, the efficacy may vary due to differing levels of antigen expression in tumors. For example, *in situ* tumor vaccines generated using tumor residues as tumor-related antigens after ablation therapy can induce anti-tumor immune responses against broad-spectrum solid drugs.[53–55] The traditional whole cancer cell vaccine method involved reinjecting lysates extracted from dissected tumor tissue into the patient's body to generate an immune response.[58] This method of photothermal-induced *in situ* vaccine-like functionality does not require complex procedures and raises no ethical issues. The tumor residues generated by photothermal tumor ablation and the nanoadjuvants in locally targeted primary tumors have a synergistic effect, effectively stimulating strong immune responses. Compared with T cell therapy or DC therapy which currently requires advanced technology and high costs,[59–64] the developed system was significantly simpler and less expensive. Normal liver and kidney function in all mice groups indicated that the synergistic FA-NPs based on PTT was safe and low toxicity. Finally, although the penetration depth of light in tissues may be limited with near-infrared lasers, clinical devices based on endoscopes with built-in lasers can be used for laser treatment of tumors localized deep in the body. Therefore, the clinical and translational nanoparticles and proposed technology may indeed be realistically applied.

The nanoparticles developed in this study offer several distinct advantages over conventional immunotherapy, which are primarily manifested in the following ways: These nanoparticles can precisely identify and specifically target cancer cells for destruction while minimizing effects on healthy cells. The immune response tailored to the tumor can suppress the growth of secondary tumors, and due to immunological memory, it provides long-term protection against tumor recurrence. The nanoparticles significantly boost the presentation of tumor antigens, thereby activating $CD8^+$ T cells, which are crucial for immune surveillance and elimination of cancer cells. The nanoparticles increase antigen presentation, strengthens the activation of T cells, and enhances T cells ability to recognize and destroy tumor cells. The nanoparticles protect immunotherapeutic agents (antigens/adjuvants) from premature degradation in the biological environment, thereby enhancing the stability of the antigens within the body. With a high drug-loading capacity, the nanoparticles can continuously and slowly release antigens, which help to increase the intensity of the immune response. Extended exposure to antigens also induces effective immune memory responses, which is vital for long-term protection against cancer. These advantages highlight the significant potential and promising prospects of nanoparticles in breast cancer immunotherapy, offering a more precise and potent treatment strategy.

In this study, a cutting-edge, dual-functional nanotech strategy has been presented. Upon exposure to NIR light, nanoparticles enriched with ginsenoside Rg3 and R837 targeted and killed breast cancer cells and reversed the suppressive TME by an effective antigen presentation process. In conclusion, the study proposed a treatment strategy that is expected to achieve clinical application for breast cancer-targeted diagnosis and treatment in the future.

Limitations of the study

The nanoparticles prepared in this study have some limitations. Given the intricate nature of the TME and the heterogeneity across various types of tumors, this research has concentrated on the clinical application of nanoparticles, specifically within the context of breast cancer. It underscores the imperative to develop tailored modifications and drug-loading strategies that can be customized to accommodate the unique needs of

Figure 6. Immune responses assessment *in vivo*

(A–C) Groups of 4T1-bearing mice were given tail vein injections three times with various formulations and sacrificed at day 15 for analysis. Six groups from left to right are PBS, PEG-PLGA, R837, FA-NPs, NPs+ NIR, and FA-NPs +NIR. (A) Representative flow cytometry plots illustrated CD4, CD8+T cells in peripheral blood; (B) Qualification of CD4, CD8+T cells according to (A), Data are represented as mean ± SEM; (C) Representative flow cytometry plots of $CD80^+$ or $CD86^+$ among CD11c+ DCs extracted from the popliteal LNs (tumor sentinel lymph nodes).

(D) Qualification of $CD80^+$ or $CD86^+$ expressions gated by CD11c + cells according to (C), data are represented as mean ± SEM.

(E) TUNEL staining of tumor slices in each group.

(F) Qualification according to (E).

(G) Representative immunofluorescence staining for $CD8^+$ (Green) of tumor sections obtained after aforementioned treatments, while the nucleus was stained with DAPI (blue), data are represented as mean ± SEM.

(H) Cytokine levels in sera from mice isolated at 24 h post different treatments, data are represented as mean ± SEM.

(I) Tumor growth curves of different groups of mice (5 mice per group) with s.c. inoculation of secondary 4T1. Data are represented as mean ± SEM.

(J) Morbidity-free survival of different groups of mice with secondary 4T1 tumors after various treatments indicated to eliminate their primary tumors (10 mice per group). $^*p < 0.05$, $^{**}p < 0.01$, and $^{***}p < 0.001$. Scale bars, 50 μm.

different tumor types and individual patient profiles. While nanoparticles have demonstrated promising biocompatibility *in vivo*, there is a pressing need for further investigation into their biosafety, particularly regarding their impact on healthy organs. In light of the challenges associated with scaling up production, the development of a robust and efficient manufacturing process for multifunctional nanoparticles remains an area that warrants further exploration and innovation.

RESOURCE AVAILABILITY

Lead contact

Further information and requests for resources and reagents should be directed to and will be fulfilled by the lead contact, Meng Wu (wb000713@whu.edu.cn).

Materials availability

This study did not generate unique reagents.

Data and code availability

- All data reported in this paper will be shared by the lead contact upon request.
- This paper does not report original code.
- Any additional information required to reanalyze the data reported in this paper is available from the lead contact upon request.

ACKNOWLEDGMENTS

We would like to thank all the editors and reviewers for their hard work, all the authors for their efforts, as well as Bullet Edits Limited for language editing and proofreading of the manuscript. We would like to express our great appreciation to Carli Yip of Seattle, USA for comments and language suggestions on our paper.

This work was supported by:

1. Key Project for Teaching Research of the Medical Department of Wuhan University (2024ZD21).
2. Key R&D Project of Hubei Province (2023BCB024).

AUTHOR CONTRIBUTIONS

C.H. and M.W., conceptualization, methodology, software, formal analysis, investigation, data curation, resources, writing—original draft, writing—review and editing, visualization and supervision; Q.K., Y.J., M.W., Y.C., and Q.Z., conceptualization, methodology, investigation, writing—review and editing; Ziming Wu. and Ziling Wu., conceptualization and writing—review and editing; S.N. and C.L., conceptualization, methodology, software, formal analysis, resources, writing—review and editing.

DECLARATION OF INTERESTS

The authors declare no competing interests.

STAR★METHODS

Detailed methods are provided in the online version of this paper and include the following:

- KEY RESOURCES TABLE
- EXPERIMENTAL MODEL AND STUDY PARTICIPANT DETAILS
  - Establishment of mice model for 4T1 subcutaneous tumorigenesis
- METHOD DETAILS
  - Synthesis of nanoparticles
  - Characterization of nanoparticles
  - *In vitro* targeted analysis
  - Drug release experiment and drug loading
  - Cell culture and cytotoxicity assay
  - Animal experiments
  - *In vivo* imaging of mice
  - Detection of immune response in mice by flow cytometry
- QUANTIFICATION AND STATISTICAL ANALYSIS
- ADDITIONAL RESOURCES

Received: October 25, 2024
Revised: December 11, 2024
Accepted: March 18, 2025
Published: March 22, 2025

REFERENCES

1. Siegel, R.L., Miller, K.D., Fuchs, H.E., and Jemal, A. (2021). Cancer statistics. CA Cancer J. Clin. *71*, 7–33.
2. Liang, S., Deng, X., Ma, P., Cheng, Z., and Lin, J. (2020). Recent Advances in Nanomaterial-Assisted Combinational Sonodynamic Cancer Therapy. Adv. Mater. *32*, e2003214.
3. Zhou, L., Hou, B., Wang, D., Sun, F., Song, R., Shao, Q., Wang, H., Yu, H., and Li, Y. (2020). Engineering Polymeric Prodrug Nanoplatform for Vaccination Immunotherapy of Cancer. Nano Lett. *20*, 4393–4402.
4. Li, Z., Zhu, L., Sun, H., Shen, Y., Hu, D., Wu, W., Wang, Y., Qian, C., and Sun, M. (2020). Fluorine assembly nanocluster breaks the shackles of immunosuppression to turn the cold tumor hot. Proc. Natl. Acad. Sci. USA *117*, 32962–32969.
5. Li, W., Yang, J., Luo, L., Jiang, M., Qin, B., Yin, H., Zhu, C., Yuan, X., Zhang, J., Luo, Z., et al. (2019). Targeting photodynamic and photothermal therapy to the endoplasmic reticulum enhances immunogenic cancer cell death. Nat. Commun. *10*, 3349.
6. Gubin, M.M., Zhang, X., Schuster, H., Caron, E., Ward, J.P., Noguchi, T., Ivanova, Y., Hundal, J., Arthur, C.D., Krebber, W.J., et al. (2014). Checkpoint blockade cancer immunotherapy targets tumour-specific mutant antigens. Nature *515*, 577–581.
7. Pardoll, D.M. (2012). The blockade of immune checkpoints in cancer immunotherapy. Nat. Rev. Cancer *12*, 252–264.
8. Maude, S.L., Frey, N., Shaw, P.A., Aplenc, R., Barrett, D.M., Bunin, N.J., Chew, A., Gonzalez, V.E., Zheng, Z., Lacey, S.F., et al. (2014). Chimeric antigen receptor T cells for sustained remissions in leukemia. N. Engl. J. Med. *371*, 1507–1517.
9. Carreno, B.M., Magrini, V., Becker-Hapak, M., Kaabinejadian, S., Hundal, J., Petti, A.A., Ly, A., Lie, W.R., Hildebrand, W.H., Mardis, E.R., and Linette, G.P. (2015). A dendritic cell vaccine increases the breadth and diversity of melanoma neoantigen-specific T cells. Science *348*, 803–808.
10. Kantoff, P.W., Higano, C.S., Shore, N.D., Berger, E.R., Small, E.J., Penson, D.F., Redfern, C.H., Ferrari, A.C., Dreicer, R., Sims, R.B., et al. (2010). Sipuleucel-T immunotherapy for castration-resistant prostate cancer. N. Engl. J. Med. *363*, 411–422.
11. Ledford, H. (2013). Immunotherapy's cancer remit widens. Nature *497*, 544.
12. Ledford, H. (2015). Therapeutic cancer vaccine survives biotech bust. Nature *519*, 17–18.
13. DeFrancesco, L. (2014). CAR-T cell therapy seeks strategies to harness cytokine storm. Nat. Biotechnol. *32*, 604.
14. Brinkman, J.A., Fausch, S.C., Weber, J.S., and Kast, W.M. (2004). Peptide-based vaccines for cancer immunotherapy. Expet Opin. Biol. Ther. *4*, 181–198.
15. Goldberg, M.S. (2019). Improving cancer immunotherapy through nanotechnology. Nat. Rev. Cancer *19*, 587–602.
16. Pu, K., Shuhendler, A.J., Jokerst, J.V., Mei, J., Gambhir, S.S., Bao, Z., and Rao, J. (2014). Semiconducting polymer nanoparticles as photoacoustic molecular imaging probes in living mice. Nat. Nanotechnol. *9*, 233–239.

17. Li, J., Yu, X., Jiang, Y., He, S., Zhang, Y., Luo, Y., and Pu, K. (2021). Second Near-Infrared Photothermal Semiconducting Polymer Nanoadjuvant for Enhanced Cancer Immunotherapy. Adv. Mater. *33*, e2003458.

18. Jaque, D., Martínez Maestro, L., del Rosal, B., Haro-Gonzalez, P., Benayas, A., Plaza, J.L., Martín Rodríguez, E., and García Solé, J. (2014). Nanoparticles for photothermal therapies. Nanoscale *6*, 9494–9530.

19. Qi, L.W., Wang, C.Z., and Yuan, C.S. (2011). Ginsenosides from American ginseng: chemical and pharmacological diversity. Phytochemistry *72*, 689–699.

20. Wang, Y.Z., Xu, Q., Wu, W., Liu, Y., Jiang, Y., Cai, Q.Q., Lv, Q.Z., and Li, X.Y. (2018). Brain transport profles of ginsenoside rb1 by glucose transporter 1: *in vitro* and *in vivo*. Front. Pharmacol. *9*, 398.

21. Hong, C., Liang, J., Xia, J., Zhu, Y., Guo, Y., Wang, A., Lu, C., Ren, H., Chen, C., Li, S., et al. (2020). One Stone Four Birds: A Novel Liposomal Delivery System Multi-functionalized with Ginsenoside Rh2 for Tumor Targeting Therapy. Nano-Micro Lett. *12*, 129.

22. Xia, J., Chen, C., Dong, M., Zhu, Y., Wang, A., Li, S., Zhang, R., Feng, C., Jiang, X., Xu, X., and Wang, J. (2023). Ginsenoside Rg3 endows liposomes with prolonged blood circulation and reduced accelerated blood clearance. J. Contr. Release *364*, 23–36.

23. Wang, Y.Z., Xu, Q., Wu, W., Liu, Y., Jiang, Y., Cai, Q.Q., Lv, Q.Z., and Li, X.Y. (2018). Brain transport profles of ginsenoside rb1 by glucose transporter 1: *in vitro* and *in vivo*. Front. Pharmacol. *9*, 398. https://doi.org/10.3389/fphar.2018.00398.

24. Chang, T.C., Huang, S.F., Yang, T.C., Chan, F.N., Lin, H.C., and Chang, W.L. (2007). Efect of ginsenosides on glucose uptake in human caco-2 cells is mediated through altered na+/glucose cotransporter 1 expression. J. Agric. Food Chem. *55*, 1993–1998.

25. Medina, R.A., and Owen, G.I. (2002). Glucose transporters: expression, regulation and cancer. Biol. Res. *35*, 9–26.

26. Liu, F., Chen, Y., Li, Y., Guo, Y., Cao, Y., Li, P., Wang, Z., Gong, Y., and Ran, H. (2018). Folate-receptor-targeted laser-activable poly(lactide-co-glycolic acid) nanoparticles loaded with paclitaxel/indocyanine green for photoacoustic/ultrasound imaging and chemo/photothermal therapy. Int. J. Nanomed. *13*, 5139–5158.

27. Lu, F., Li, Z., Sheng, Y., Ma, Y., Yang, Y., Ren, Y., Su, Z., Yu, R., and Zhang, S. (2021). Thermal-triggered packing of lipophilic NIR dye IR780 in hepatitis B core at critical ionic strength and cargo-host ratio for improved stability and enhanced cancer phototherapy. Biomaterials *276*, 121035.

28. Song, J., Zhang, N., Zhang, L., Yi, H., Liu, Y., Li, Y., Li, X., Wu, M., Hao, L., Yang, Z., and Wang, Z. (2019). IR780-loaded folate-targeted nanoparticles for near-infrared fluorescence image-guided surgery and photothermal therapy in ovarian cancer. Int. J. Nanomed. *14*, 2757–2772.

29. Xu, S., Feng, Z., Zhang, Y., Ni, H., Liu, Z., and Wang, D. (2022). pH-responsive Astragalus polysaccharide-loaded PLGA nanoparticles as an adjuvant system to improve immune responses. Int. J. Biol. Macromol. *222*, 1936–1947.

30. Chen, C., Ke, J., Zhou, X.E., Yi, W., Brunzelle, J.S., Li, J., Yong, E.L., Xu, H.E., and Melcher, K. (2013). Structural basis for molecular recognition of folic acid by folate receptors. Nature *500*, 486–489.

31. Assaraf, Y.G., Leamon, C.P., and Reddy, J.A. (2014). The folate receptor as a rational therapeutic target for personalized cancer treatment. Drug Resist. Updates *17*, 89–95.

32. Miao, Q., Xie, C., Zhen, X., Lyu, Y., Duan, H., Liu, X., Jokerst, J.V., and Pu, K. (2017). Molecular afterglow imaging with bright, biodegradable polymer nanoparticles. Nat. Biotechnol. *35*, 1102–1110.

33. Schudel, A., Francis, D.M., and Thomas, S.N. (2019). Material design for lymph node drug delivery. Nat. Rev. Mater. *4*, 415–428.

34. Lu, Q., Kou, D., Lou, S., Ashrafizadeh, M., Aref, A.R., Canadas, I., Tian, Y., Niu, X., Wang, Y., Torabian, P., et al. (2024). Nanoparticles in tumor microenvironment remodeling and cancer immunotherapy. J. Hematol. Oncol. *17*, 16.

35. Veider, F., Sanchez Armengol, E., and Bernkop-Schnürch, A. (2024). Charge-Reversible Nanoparticles: Advanced Delivery Systems for Therapy and Diagnosis. Small *20*, e2304713.

36. Sun, M., Li, Y., Zhang, W., Gu, X., Wen, R., Zhang, K., Mao, J., Huang, C., Zhang, X., Nie, M., et al. (2023). Allomelanin-based biomimetic nanotherapeutics for orthotopic glioblastoma targeted photothermal immunotherapy. Acta Biomater. *166*, 552–566.

37. Yuan, Z., He, H., Zou, J., Wang, H., Chen, Y., Chen, Y., Lan, M., Zhao, Y., and Gao, F. (2023). Polydopamine-coated ferric oxide nanoparticles for R848 delivery for photothermal immunotherapy in breast cancer. Int. J. Pharm. *644*, 123249.

38. Wu, X., Suo, Y., Shi, H., Liu, R., Wu, F., Wang, T., Ma, L., Liu, H., and Cheng, Z. (2020). Deep-Tissue Photothermal Therapy Using Laser Illumination at NIR-IIa Window. Nano-Micro Lett. *12*, 38.

39. Frigo, L., Luppi, J.S.S., Favero, G.M., Maria, D.A., Penna, S.C., Bjordal, J.M., Bensadoun, R.J., and Lopes-Martins, R.A.B. (2009). The effect of low-level laser irradiation (In-Ga-Al-AsP - 660 nm) on melanoma in vitro and in vivo. BMC Cancer *9*, 404.

40. Li, G., Zhang, J., Zhang, S., Teng, L., and Sun, F. (2023). Multifunctional nanoadjuvant-driven microenvironment modulation for enhanced photothermal immunotherapy in breast cancer. J. Contr. Release *362*, 309–324.

41. Perez-Penco, M., Byrdal, M., Lara de la Torre, L., Ballester, M., Khan, S., Siersbæk, M., Lecoq, I., Madsen, C.O., Kjeldsen, J.W., Svane, I.M., and Hansen, M. (2024). The antitumor activity of TGFβ-specific T cells is dependent on IL-6 signaling. Cell. Mol. Immunol. *22*, 111–126.

42. Yi, M., Li, T., Niu, M., Zhang, H., Wu, Y., Wu, K., and Dai, Z. (2024). Targeting cytokine and chemokine signaling pathways for cancer therapy. Signal Transduct. Targeted Ther. *9*, 176.

43. Mirlekar, B., and Pylayeva-Gupta, Y. (2021). IL-12 Family Cytokines in Cancer and Immunotherapy. Cancers *13*, 167.

44. Shan, X., Fu, Y.S., Aziz, F., Wang, X.Q., Yan, Q., and Liu, J.W. (2014). Ginsenoside Rg3 Inhibits Melanoma Cell Proliferation through Down-Regulation of Histone Deacetylase 3 (HDAC3) and Increase of p53 Acetylation. PLoS One *9*, 0115401.

45. Xia, J., Zhang, S., Zhang, R., Wang, A., Zhu, Y., Dong, M., Ma, S., Hong, C., Liu, S., Wang, D., and Wang, J. (2022). Targeting therapy and tumor microenvironment remodeling of triplenegative breast cancer by ginsenoside Rg3 based liposomes. J. Nanobiotechnol. *20*, 414.

46. Wang, J.H., Nao, J.F., Zhang, M., and He, P. (2014). 20(s)-ginsenoside Rg3 promotes apoptosis in human ovarian cancer HO-8910 cells through PI3K/Akt and XIAP pathways. Tumour Biol. *35*, 11985–11994.

47. Rahimi, S., van Leeuwen, D., Roshanzamir, F., Pandit, S., Shi, L., Sasanian, N., Nielsen, J., Esbjörner, E.K., and Mijakovic, I. (2023). Ginsenoside Rg3 Reduces the Toxicity of Graphene Oxide Used for pH-Responsive Delivery of Doxorubicin to Liver and Breast Cancer Cells. Pharmaceutics *15*, 391.

48. Zhu, Y., Wang, A., Zhang, S., Kim, J., Xia, J., Zhang, F., Wang, D., Wang, Q., and Wang, J. (2023). Paclitaxel-loaded ginsenoside Rg3 liposomes for drug-resistant cancer therapy by dual targeting of the tumor microenvironment and cancer cells. J. Adv. Res. *49*, 159–173.

49. Sun, D., Zou, Y., Song, L., Han, S., Yang, H., Chu, D., Dai, Y., Ma, J., O'Driscoll, C.M., Yu, Z., and Guo, J. (2022). A cyclodextrinbased nanoformulation achieves co-delivery of ginsenoside Rg3 and quercetin for chemo-immunotherapy in colorectal cancer. Acta Pharm. Sin. B *12*, 378–393.

50. Liu, X., Zhang, Z., Liu, J., Wang, Y., Zhou, Q., Wang, S., and Wang, X. (2019). Ginsenoside Rg3 improves cyclophosphamide- induced immunocompetence in Balb/c mice. Int. Immunopharmacol. *72*, 98–111.

51. Jiang, Z., Yang, Y., Yang, Y., Zhang, Y., Yue, Z., Pan, Z., and Ren, X. (2017). Ginsenoside Rg3 attenuates cisplatin resistance in lung cancer by downregulating PD-L1 and resuming immune. Biomed. Pharmacother. *96*, 378–383.

52. Chen, Q., Xu, L., Liang, C., Wang, C., Peng, R., and Liu, Z. (2016). Photothermal therapy with immune-adjuvant nanoparticles together with checkpoint blockade for effective cancer immunotherapy. Nat. Commun. *7*, 13193.

53. Chen, B., Huang, R., Zeng, W., Wang, W., and Min, Y. (2024). Nanocodelivery of an NIR photothermal agent and an acid-responsive TLR7 agonist prodrug to enhance cancer photothermal immunotherapy and the abscopal effect. Biomaterials *305*, 122434.

54. Huang, J., Leng, X., Jiang, T., Xu, L., Zheng, J., Fang, M., Wang, J., Wang, Z., and Zhang, L. (2023). Oxygen-carrying nanoplatform to reprogram tumor immunosuppressive microenvironment and enhance photothermal-immunotherapy. Mater. Today. Bio *19*, 100555.

55. Zheng, J., Huang, J., Zhang, L., Wang, M., Xu, L., Dou, X., Leng, X., Fang, M., Sun, Y., and Wang, Z. (2023). Drug-loaded microbubble delivery system to enhance PD-L1 blockade immunotherapy with remodeling immune microenvironment. Biomater. Res. *27*, 9.

56. Mottas, I., Bekdemir, A., Cereghetti, A., Spagnuolo, L., Yang, Y.S.S., Müller, M., Irvine, D.J., Stellacci, F., and Bourquin, C. (2019). Amphiphilic nanoparticle delivery enhances the anticancer efficacy of a TLR7 ligand via local immune activation. Biomaterials *190*, 111–120.

57. Wang, L., He, Y., He, T., Liu, G., Lin, C., Li, K., Lu, L., and Cai, K. (2020). Lymph node-targeted immune-activation mediated by imiquimod-loaded mesoporous polydopamine based-nanocarriers. Biomaterials *255*, 120208.

58. Krishnan, N., Jiang, Y., Zhou, J., Mohapatra, A., Peng, F.X., Duan, Y., Holay, M., Chekuri, S., Guo, Z., Gao, W., et al. (2024). A modular approach to enhancing cell membrane-coated nanoparticle functionality using genetic engineering. Nat. Nanotechnol. *19*, 345–353.

59. Binnewies, M., Roberts, E.W., Kersten, K., Chan, V., Fearon, D.F., Merad, M., Coussens, L.M., Gabrilovich, D.I., Ostrand-Rosenberg, S., Hedrick, C.C., et al. (2018). Understanding the tumor immune microenvironment (TIME) for effective therapy. Nat. Med. *24*, 541–550.

60. Galon, J., and Bruni, D. (2019). Approaches to treat immune hot, altered and cold tumours with combination immunotherapies. Nat. Rev. Drug Discov. *18*, 197–218.

61. Topalian, S.L., Taube, J.M., Anders, R.A., and Pardoll, D.M. (2016). Mechanism-driven biomarkers to guide immune checkpoint blockade in cancer therapy. Nat. Rev. Cancer *16*, 275–287.

62. Wang, Y., Xiang, Y., Xin, V.W., Wang, X.W., Peng, X.C., Liu, X.Q., Wang, D., Li, N., Cheng, J.T., Lyv, Y.N., et al. (2020). Dendritic cell biology and its role in tumor immunotherapy. J. Hematol. Oncol. *13*, 107.

63. Tacken, P.J., de Vries, I.J.M., Torensma, R., and Figdor, C.G. (2007). Dendritic-cell immunotherapy: from ex vivo loading to *in vivo* targeting. Nat. Rev. Immunol. *7*, 790–802.

64. Curran, M.A., Montalvo, W., Yagita, H., and Allison, J.P. (2010). PD-1 and CTLA-4 combination blockade expands infiltrating T cells and reduces regulatory T and myeloid cells within B16 melanoma tumors. Proc. Natl. Acad. Sci. USA *107*, 4275–4280.

STAR★METHODS

KEY RESOURCES TABLE

REAGENT or RESOURCE	SOURCE	IDENTIFIER
Chemicals, peptides, and recombinant proteins		
IR780	MCE	Cat. No. 207399-07-3
imiquimod (R837)	MCE	Cat. No. 99011-02-6
Ginsenoside Rg3	Shanghai Xushuo Biotechnology Co., Ltd	Cat. No. 14197-60-5
DiI (1,1′- dioctyl-3,3,3', 3′- tetramethylindocyanine perchlorate)	Sigma-Aldrich	Cat. No. 42364
DAPI (4′, 6-diamino-2-phenylindole)	Sigma-Aldrich	Cat. No. D9542
carboxyl PLGA (COOH-PLGA)	Daigang Biomaterial	Cat. No. DG-50DLGH018
Methoxy-PEG-PLGA	Daigang Biomaterial	N/A
amino PEG amino (NH2-PEG-NH2)	Daigang Biomaterial	N/A
Molecular biology grade agarose	Thermo Fisher Scientific	Cat. No. 17850
DiR (1,1′- dioctyl-3,3,3', 3′- tetramethylindole tricarbocyanine iodide)	Thermo Fisher Scientific	Cat. No. D12731
PFH (Perfluorohexane)	Apollo Scientific	N/A
Anti-CTLA4	Bioxcell	Cat. No. BE0164; RRID: AB_10950184
APC/Cyanine7 anti-mouse CD3 Antibody	BioLegend	Cat. No. 100221; RRID: AB_2057374
APC anti-mouse CD8a Antibody	BioLegend	Cat. No. 100711 ; RRID: AB_312751
APC anti-mouse CD11c Antibody	BioLegend	Cat. No. 117309; RRID: AB_313778
FITC anti-mouse CD80 Antibody	BioLegend	Cat. No. 104705; RRID: AB_313127
PE anti-mouse CD86 Antibody	BioLegend	Cat. No. 105105; RRID: AB_313159
Folic Acid-FITC Conjugate (FA-FITC)	Hapten and Protein Biomedical Institute	Cat. No. 4610012-F
Anti-CD8 alpha antibody	Abcam	Cat. No. ab316778; RRID: AB_443686
EXPERIMENTAL MODEL AND STUDY PARTICIPANT DETAILS		
4T1 cells (mouse)	This laboratory	(RRID: CVCL_0125)
Experimental models: Organisms/strains		
BALB/c (six-week-old)	This laboratory	(RRID: Strain code_211)
Software and algorithms		
SPSS 21.0 software	Norman H et al.	https://www.ibm.com
GraphPad Prism (version 8.0)	GraphPad Software, La Jolla California, USA	https://www.graphpad.com/

EXPERIMENTAL MODEL AND STUDY PARTICIPANT DETAILS

Establishment of mice model for 4T1 subcutaneous tumorigenesis

An animal model for subcutaneous tumorigenesis was developed using six-week-old Female BALB/c mice, with all experimental protocols adhering to the ethical standards set by the Animal Care and Use Committee at Wuhan University. Following 2 weeks habituation, 4T1 tumor cells (5×10^5) were injected into the left flank of the mice to initiate tumorigenesis. The cell lines were tested for mycoplasma contamination, there was no mycoplasma contamination for 4T1 cells.

METHOD DETAILS

Synthesis of nanoparticles

Various proportions of PEG-PLGA, IR780, R837, ginsenoside Rg3, and PFH were combined in a 2 mL dichloromethane solution to formulate an organic phase. An ultrasonic homogenizer (VCX130; Sonics and Materials, Newton, CT, USA) was then applied to emulsify the mixture at 100W for 6 min, employing an intermittent sonication pattern (5 s of activity followed by 5-s pause). Subsequently, 8 mL of a 5% polyvinyl alcohol solution was added, and the emulsification process was further carried out for 4 min at 50W, maintaining the intermittent pattern. The nanoparticles shell formation was achieved through the evaporation of dichloromethane, with this

step conducted in an ice bath to control the temperature. To remove any surplus reagents, the emulsion was centrifuged at 10,000 rpm for 5 min and subsequently washed with PBS. This sequence of centrifugation and washing was iterated three times to ensure thorough purification. The final NP product was stored at a temperature of 4°C. For the preparation of folate-conjugated nanoparticles (FA-NPs), the initial steps were analogous, with the subsequent integration of an incubation phase to facilitate binding with folate receptors. This was preceded by a pre-incubation of the NPs in a BSA solution to block non-specific binding sites. The NPs were then exposed to folate antibodies for a period of 4 h at room temperature, using an orbital shaker to maintain gentle agitation. Post-incubation, the NPs were pelleted by centrifugation at 10,000 rpm for 5 min, and a PBS washing regimen was repeated 3 times to ensure the removal of unbound antibodies and to preserve the integrity and functionality of the FA-NPs.

Characterization of nanoparticles

The size and surface charge of both NPs and FA-NPs were characterized using dynamic light scattering with a Zetasizer Nano ZS90 (Malvern Instruments, Malvern, UK). The process commenced with the dilution of both NPs and FA-NPs dispersions in ultrapure water to ensure optical clarity. Following this, the morphological assessment of the FA-NPs was performed using scanning electron microscopy (SEM), providing detailed insights into their structure.

In vitro targeted analysis

To determine the folic acid binding capacity of FA-NPs, the FA targeting on FA-NPs was labeled with FA-FITC. For the fluorescent labeling of PLGA nanoparticles, we introduced either 1 mg of DiI or DiR dyes into the organic phase, maintaining all subsequent preparation steps as per the standard protocol. The FA-NPs were then observed using a confocal laser-scanning microscope (CLSM; A1R-Si; Nikon, Tokyo, Japan).

Drug release experiment and drug loading

To evaluate the effect of FA-NPs based on near-infrared laser, an *in vitro* experiment was designed to detect the release of ginsenoside Rg3 and TLR7. Equal aliquots of the FA-NPs suspension were loaded into individual dialysis bags with a 7kDa molecular weight cutoff. The encapsulation efficiency of R837 was determined using10kDa. These bags were submerged in a 150 mL container filled with a buffer solution (30% ethanol, 0.01% Tween, 0.02% sodium azide, pH 7.4) and set in a shaking water bath at 100 rpm and 37°C. At intervals of 1, 4, 8, 12, and 24 h, 1 mL samples were extracted from the buffer and immediately replaced with fresh buffer. The experimental group was treated by removing the bag and exposing it to an 808 nm NIR laser at a power density of 1W/cm^2 for 5 min. The dialysis process for the treated group was then continued in the same manner as the control. The samples collected were assessed using HPLC to ascertain the cumulative release of ginsenoside Rg3/TLR7. The HPLC analysis was conducted using a Shimadzu system, equipped with dual 510 pumps and a UV spectrophotometric detector (Shimadzu C-20; Japan). For the separation and analysis of the ginsenoside-containing product mixtures, 20 mL samples were passed through a 5.0-micron 120-5-C18-ace-EPS column (250 mm × 4.6 mm, Pronto Sil; Germany) maintained at a temperature of 30°C. The mobile phase composition was meticulously adjusted as follows: a gradient from 15% to 34.5% acetonitrile in distilled water over the first 10 min, increasing to 47.5% between 10 and 25 min, then to 80% between 25 and 40 min, followed by a shift to 100% from 40 to 50 min, holding at 100% until 55 min, and finally returning to 15% from 55 to 56 min. The flow rate was consistently maintained at 1.0 mL/min. For the detection of ginsenosides, the absorbance was monitored at 203 nm, while for Imiquimod, it was set at 220 nm. Chromatographic peaks were identified by comparing their retention times with those of known reference standards. The encapsulation efficiency of ginsenoside Rg3/TLR7 within the nanoparticles was determined by the following formula:

Encapsulation Efficiency = (Mass of Encapsulated drug/Total Mass of drug Added) ×100%.

Cell culture and cytotoxicity assay

4T1 breast cancer cells were cultivated in DMEM (10% FBS) under 37°C with 5% CO_2. 4T1 cells (5×10^3 cells/well in 100 μL) were seeded into a 96-well plate and subjected to drugs for 4 h. The wells were then thoroughly washed with PBS, and 100 μL of fresh medium was introduced. The cells underwent irradiation with an 808 nm near-infrared laser at a power density of 1 W/cm^2 for 2 min, followed by incubation for either 24, 48, or 72 h. Cell viability was determined using the CCK8 assay, where 10% CCK8 reagent in the fresh medium was added, and the plates were incubated for 2 h before the absorbance at 450 nm was recorded using a microplate reader (ELX800; BioTek Instruments, Winooski, VT, USA).

Animal experiments

Female BALB/c mice were administered various drug solutions intravenously at standardized doses (n = 5). Subsequently, the mice bearing tumors were divided into 6 cohorts (n = 5 per group): FA-IR780-R837-Ginsenoside Rg3-PFH@PEG-PLGA NPs + NIR (FA-NPs + NIR), IR780-R837-Ginsenoside Rg3-PFH@PEG-PLGA NPs + NIR (NPs + NIR), FA-IR780-R837- Ginsenoside Rg3-PFH@PEG-PLGA NPs (FA-NPs), PEG-PLGA, R837, and PBS. Each group was injected intravenously with the NPs solution, R837, or PBS at a dosage of 50 mg/kg in a volume of 200 μL. An hour post-injection, the tumor areas were irradiated with an 808 nm near-infrared laser at a power density of 1 W/cm^2 for 5 min. Tumor size and mass were assessed every 3 days, with the volume calculated using the formula $V = L\times W^2/2$, where L denotes the length and W denotes the width. On the third day after irradiation, mice from each group were euthanized by cervical dislocation, their tumors were extracted, fixed, and then underwent immunohistochemical

staining. On the seventh day post-administration, blood was collected for assessing liver and kidney functions, and the mice were euthanized via cervical dislocation. In the anti-secondary tumors experiment, 4T1 cells (5×10^5) suspended in phosphate-buffered saline (PBS) were administered subcutaneously into the right flank region of each female BALB/c mouse which took place seven days afterward. Mice were given intravenous injections of 10 mg anti-CTLA4 in 0.2 mL PBS on days 1, 4, and 7. After the primary tumors were eliminated using photothermal therapy or surgical resection, the development of secondary tumors was closely monitored.

In vivo imaging of mice

Tumor-bearing mice were randomly allocated to two groups (n = 5 per group) and administered an intravenous injection of DIR-labeled FA-NPs or NPs at a dosage of 50 mg/kg in a volume of 200 μL. The Xenogen IVIS spectral imaging system (PerkinElmer) was utilized to acquire fluorescent images following injection. The mice were humanely euthanized by cervical dislocation, and the principal organs (heart, liver, spleen, lungs, and kidney, as well as the tumor tissue) were scrutinized using fluorescence imaging. In the context of photoacoustic imaging, tumor tissues were visualized at multiple time points preceding and succeeding the introduction of FA-NPs and NPs. Ultrasound imaging was applied to record the tumor tissues before and after laser exposure.

Detection of immune response in mice by flow cytometry

To study the immune response induced by the above treatment, a 4T1 breast cancer mice tumor model was constructed, and blood was randomly drawn from each group of mice. PBMC single-cell suspensions were separated and labeled with fluorescein flow cytometry antibodies. Immune cells were harvested from mice blood and lymph nodes in each group. Immune cells were stained with fluorescence-labeled antibodies after the removal of red blood cells (RBC) using the RBC lysis buffer. Lymph node tissues were cut into small pieces and single-cell suspensions were made using a glass homogenizer containing PBS (pH 7.4) with 2% heat-inactivated fetal bovine serum. Cytokine levels were measured by ELISA. In addition, the sliced tumors were stained with CD8 and TUNEL and then observed under a CLSM.

QUANTIFICATION AND STATISTICAL ANALYSIS

Data were presented as the mean ± standard deviation (SD). Data comparison of two groups was carried out by Student's t test. The graphs were plotted using the GraphPad Prism 8.0 software (GraphPad Software, CA, USA). Independent samples were used for inter-group comparison, and one-way ANOVA was performed using SPSS 21.0 software. $^{*}p < 0.05$, $^{**}p < 0.01$, $\#p < 0.001$, and $^{***}p < 0.001$ was considered significant.

ADDITIONAL RESOURCES

The work is not part of/involves a clinical trial.